Research article

Quantitative magnetization transfer imaging of rodent glioma using selective inversion recovery

Junzhong Xu[a,b]*, Ke Li[a,b], Zhongliang Zu[a,b], Xia Li[a,b], Daniel F. Gochberg[a,b,c] and John C. Gore[a,b,c,d,e]

Magnetization transfer (MT) provides an indirect means to detect noninvasively variations in macromolecular contents in biological tissues, but, so far, there have been only a few quantitative MT (qMT) studies reported in cancer, all of which used off-resonance pulsed saturation methods. This article describes the first implementation of a different qMT approach, selective inversion recovery (SIR), for the characterization of tumor *in vivo* using a rodent glioma model. The SIR method is an on-resonance method capable of fitting qMT parameters and T_1 relaxation time simultaneously without mapping B_0 and B_1, which is very suitable for high-field qMT measurements because of the lower saturation absorption rate. The results show that the average pool size ratio (PSR, the macromolecular pool *versus* the free water pool) in rat 9 L glioma (5.7%) is significantly lower than that in normal rat gray matter (9.2%) and white matter (17.4%), which suggests that PSR is potentially a sensitive imaging biomarker for the assessment of brain tumor. Despite being less robust, the estimated MT exchange rates also show clear differences from normal tissues (19.7 Hz for tumors *versus* 14.8 and 10.2 Hz for gray and white mater, respectively). In addition, the influence of confounding effects, e.g. B_1 inhomogeneity, on qMT parameter estimates is investigated with numerical simulations. These findings not only help to better understand the changes in the macromolecular contents of tumors, but are also important for the interpretation of other imaging contrasts, such as chemical exchange saturation transfer of tumors. Copyright © 2013 John Wiley & Sons, Ltd.

Keywords: quantitative magnetization transfer; selective inversion recovery; pool size ratio; exchange rate; chemical exchange; cancer; 9 L

INTRODUCTION

In general, magnetization transfer (MT) describes the spin exchange processes between nuclei in different environments, but MT imaging is usually interpreted as exchange between macromolecular and free water proton pools via dipolar interactions and/or chemical exchange. The magnetization transfer ratio (MTR) (1) has been defined as a semi-quantitative metric of the contrast available from simple MT weighting of MRI signals. The macromolecular proton signal is largely invisible in conventional MRI acquisitions, and so the MTR provides an indirect measurement of macromolecular contents in biological tissues. The macromolecular content of tissues varies during the progression of several diseases. Therefore, MTR imaging has been successfully applied to, for example, neurological disorders (2), liver fibrosis (3), neuromuscular diseases (4) and cancer (5–9).

Although MTR has been found to be useful in practice and to correlate with various pathological changes, MTR values are also sensitive to various experimental parameters, including the radiofrequency (RF) irradiation power, frequency offset and tissue relaxation properties, which reduce the specificity to changes in macromolecular contents. More importantly, these confounding parameters are user specific and the inability to standardize methods hinders general clinical applications, especially in large-scale, multiple-site clinical trials. Furthermore, even if MTR acquisition parameters universally adhered to a standard, as suggested previously (10,11), the MTR metric is inherently sensitive to multiple tissue properties and hence fails to distinguish between, for example, changes in the pool size ratio

(PSR), i.e. the ratio of protons in the macromolecular pool to those in the free water pool, and R_1. In order to reduce this dependence on acquisition parameters, and to increase the biophysical

* Correspondence to: J. Xu, Vanderbilt University, Institute of Imaging Science, 1161 21st Avenue South, AA 1105 MCN, Nashville, TN 37232-2310, USA. E-mail: junzhong.xu@vanderbilt.edu

a J. Xu, K. Li, Z. Zu, X. Li, D. F. Gochberg, J. C. Gore
   Institute of Imaging Science, Vanderbilt University, Nashville, TN, USA

b J. Xu, K. Li, Z. Zu, X. Li, D. F. Gochberg, J. C. Gore
   Department of Radiology and Radiological Sciences, Vanderbilt University, Nashville, TN, USA

c D. F. Gochberg, J. C. Gore
   Department of Physics and Astronomy, Vanderbilt University, Nashville, TN, USA

d J. C. Gore
   Department of Biomedical Engineering, Vanderbilt University, Nashville, TN, USA

e J. C. Gore
   Department of Molecular Physiology and Biophysics, Vanderbilt University, Nashville, TN, USA

specificity, quantitative MT (qMT) imaging has been developed to quantify intrinsic MT parameters, including relaxation rates, PSR and MT exchange rates (12–14). Several different approaches of qMT imaging have been reported, including conventional continuous-wave (12) and pulsed saturation (14) methods using RF pulses with multiple frequency offsets and/or amplitudes. Distinct from these steady-state approaches, selective inversion recovery (SIR) (13,15) is a transient, on-resonance qMT technique, in which an on-resonance RF pulse is applied to selectively invert the free water protons. The resulting transient longitudinal magnetization can be measured and fitted to a bi-exponential recovery (16), from which the intrinsic MT parameters can be estimated. Unlike conventional continuous-wave and pulsed saturation qMT methods, the SIR-qMT approach does not require extra mapping of B_0 and B_1, and, conveniently, T_1 and qMT parameters can be fitted simultaneously. The SIR technique has been applied previously to quantify MT parameters in phantoms (17), ferret (18), rat (19), human brain (20,21) and human skeletal muscles (22) *in vivo*.

In the last two decades, MTR has been widely adopted in cancer imaging, including imaging studies of cerebral (5,8), prostate (9), pancreatic (6) and breast (7) cancers. However, only a small number of studies of cancer using qMT have been reported (8,23–25), and these all used the pulsed saturation qMT method. No systematic studies of tumors have been reported previously using the SIR approach. In addition to assessing changes in macromolecular content in tumors, quantitative mapping of MT parameters may also be important to obtain a better understanding of changes relevant for other imaging methods. For example, the quantification of chemical exchange saturation transfer (CEST) imaging data suffers significantly from MT asymmetry effects on the measured signals (26), and the interpretation of CEST measurements of protein amides may be affected by whether concomitant variations occur in total protein content. In the current study, qMT measurements using the SIR approach have been applied to assess tumor characteristics for the first time using a rodent glioma model. A new SIR-echo planar imaging (EPI) sequence was developed to ensure that a minimal TR could be achieved to significantly accelerate the image acquisition. The fitted qMT parameters are consistent with previously published results. Both the PSR and MT exchange rates are potentially sensitive imaging biomarkers for the detection of tumors and the assessment of the state of tissues. In addition, maps of T_2 and apparent diffusion coefficient (ADC) were also acquired and correlated with qMT data, which may be helpful to obtain a better understanding of MT contrast in tumors.

THEORY

SIR-qMT

Biological tissues are considered to comprise two pools of protons, a free water pool (f) and a macromolecular pool (m), and each pool has unique equilibrium magnetizations ($M_{f\infty}$ and $M_{m\infty}$) and spin–lattice relaxation rates (R_{1f} and R_{1m}). MT between the pools may be modeled by adding coupling terms to the Bloch equations (17). The recovery of the free pool longitudinal magnetization $M_f(t)$ can then be described by a bi-exponential function:

$$\frac{M_f(t)}{M_{f\infty}} = b_f^+ e^{-R_1^+ t} + b_f^- e^{-R_1^- t} + 1 \tag{1}$$

where R_1^+ and R_1^- are the fast and slow recovery rates, respectively, of the overall recovery. It should be noted that R_1^- is the

conventional spin–lattice relaxation rate when measured with an inversion recovery experiment, as most studies use inversion times much greater than $1/R_1^+$. If k_{fm} is the MT exchange rate from the free to the macromolecular pool and k_{mf} is the rate in the reverse direction, all parameters in Equation [1] can be solved analytically, i.e.:

$$2R_1^{\pm} = R_{1f} + R_{1m} + k_{fm} \tag{2}$$
$$+ k_{mf} \pm \sqrt{(R_{1f} - R_{1m} + k_{fm} - k_{mf})^2 + 4k_{fm}k_{mf}}$$

and

$$b_f^{\pm} = \pm \frac{\left[\frac{S_f M_f(0^-)}{M_{f\infty}} - 1\right]\left(R_{1f} - R_1^{\mp}\right) + \left[\frac{S_f M_f(0^-)}{M_{f\infty}} - \frac{S_m M_m(0^-)}{M_{m\infty}}\right] k_{fm}}{R_1^+ - R_1^-} \tag{3}$$

where subscripts 'f' and 'm' represent free and macromolecular pools, respectively. R_{1f} and R_{1m} are the spin–lattice relaxation rates, and $M_f(0^-)$ and $M_m(0^-)$ are the magnetizations before the inversion pulse, which have experienced a longitudinal recovery with a pre-delay time t_d. It should be noted that the inversion pulse may not completely invert the longitudinal magnetization of the free pool, and may also have some influence on the macromolecular pool; therefore, two more parameters (the inversion coefficients S_f and S_m) must be introduced to account for these effects. Using Equations [1]–[3], the qMT parameters, e.g. the pool size ratio (PSR = $M_{m\infty}/M_{f\infty}$) and exchange rate k_{mf} ($k_{fm} = k_{mf} \times$ PSR), can be quantified by fitting the measured signals to a bi-exponential recovery.

SIR-EPI with saturation pulse train

SIR-qMT acquisitions were first evaluated using phantoms consisting of cross-linked bovine serum albumin, employing EPI with long TRs chosen so that long pre-delay times $t_d \approx 5\,T_1$ ensured a full recovery of $M_f(t)$ between scans (17). However, such long TRs significantly increase the total scan time, which would make this approach clinically nonfeasible. A fast spin echo (FSE) acquisition has been proposed (18), in which the longitudinal magnetizations of both the free and macromolecular pools are saturated and are approximately zero at the end of the FSE readout, so that a much shorter pre-delay time, as well as a much shorter TR, can be used. The effect of the partial recovery of $M_f(t)$ in the shorter pre-delay period can be accounted for in the signal model, so that all SIR-qMT parameters may still be quantified without bias (18). This technique significantly reduces the pre-delay time t_d and the total scan time, and has been successfully applied previously in the imaging of rat (18,19) and human brain (20) *in vivo*.

In the current study, a new SIR-EPI sequence was introduced to combine the advantages of the fast acquisition of EPI and short pre-delay time of SIR-FSE. Specifically, the EPI readout scheme that acquires qMT data was followed by a saturation pulse train consisting of multiple 180° pulses (see Fig. 1). The EPI readout ensures fast acquisitions, whilst the train of saturation pulses ensures that a short TR can be used. Such a sequence can further accelerate the acquisition of SIR-qMT experiments relative to SIR-FSE methods, but preserve the ability to estimate qMT parameters without bias. It should be noted that the TR in this sequence is dynamic and minimized in each scan to different values depending on t_i and t_d. Hence, it avoids the conventional long waiting periods when short t_i and/or t_d are used, and significantly increases the acquisition efficiency. A similar
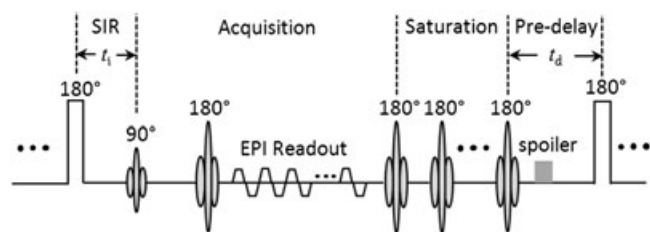
Figure 1. Diagram of selective inversion recovery-echo planar imaging (SIR-EPI) sequence with a saturation pulse train applied after the EPI readout to saturate the free and macromolecular pools.

technique of using a saturation pulse train in SIR sequences has been reported recently for human brain imaging at 7 T (21). However, that method used pulses of different flip angles (135°) and a turbo field echo readout which can slightly bias the estimation of qMT parameters (21).

MATERIALS AND METHODS

Animal preparation

9 L glioblastoma cells were obtained from the American Type Culture Collection, Manassas, VA, USA (ATCC 9 L/lacZ, CRL-2200) and grown in Dulbecco's modified Eagle's medium (Gibco, Gaithersburg, MD, USA) with 10% fetal calf serum and 500 µg/mL penicillin. Cells were maintained in a humidified incubator at 37 °C with 5% CO_2.

All animal-related procedures were approved by our institution's Animal Care and Use Committee. Eight male Fischer 344 rats (250–300 g) were immobilized and anesthetized with a 2%/98% isoflurane–oxygen mixture. The rats were inoculated with 1×10^5 9 L glioblastoma cells in 5 µL of Dulbecco's modified Eagle's medium using a 10-µL gas-tight syringe, approximately 1 mm anterior and 2 mm lateral to the bregma on the right side of the head, at a depth of 4 mm relative to the dural surface. Rats were imaged 14–18 days after intracranial inoculation depending on the size of the tumors developed. More details of these procedures have been reported previously (27).

In vivo MRI experiments

Animals were anesthetized with isoflurane (3% for induction and 2% during the imaging experiments) and fixed in an MRI-compatible cradle with bite and head bars. Rectal temperature was maintained at around 37 °C using a warm-air feedback system throughout the experiment. A birdcage RF coil with an internal diameter of 38 mm was used for both the transmitter and receiver.

All experiments were performed on a 9.4-T Agilent MRI scanner (Agilent Technologies Inc., Santa Clara, CA, USA) using a two-shot spin-echo EPI sequence (number of excitations, 2). A triple reference imaging scheme (28) was used to reduce EPI artifacts, with two phase-encoded images with reversed readout and phase-encoding directions and two corresponding non-phase-encoded phase maps. A single axial slice crossing the center of the tumor was acquired with a slice thickness of 2 mm, field of view of 32×32 mm^2 and matrix size of 96×96, yielding an isotropic in-plane resolution of 333 µm. Both the spin–lattice relaxation time T_1 and multiple qMT parameters were obtained using the SIR-EPI sequence shown in Fig. 1. Specifically, a 1-ms hard inversion pulse was applied to invert the longitudinal magnetization of the free water pool. There were 20 inversion

times used in the current study, which were logarithmically distributed over the range from 5 ms to 10 s, whilst the pre-delay time t_d was kept constant at 3.5 s. The saturation pulse train had 10 refocusing pulses with an echo spacing of 10 ms. Previous computer simulations had verified that the longitudinal magnetization would be completely saturated at the end of the echo train (18). The total scanning time for qMT measurements was less than 14 min.

In addition, maps of the spin–spin relaxation times T_2 were obtained using spin-echo EPI with multiple TEs, i.e. 30, 40, 60, 80 and 100 ms. ADC maps were obtained using a pulsed gradient spin echo sequence with a gradient duration (δ) of 5 ms and separation (Δ) of 12 ms, and fitted mono-exponentially with four b values (400, 600, 800 and 1000 s/mm^2).

Data analysis

All data analyses were performed with programs written in MATLAB (Mathworks, Natick, MA, USA). For each animal, all images were co-registered to the corresponding SIR-EPI image acquired at $t_i = 10$ s using a rigid body registration algorithm by maximizing the normalized mutual information (29). Following co-registration, the brain region was manually selected for further data fitting. All MR parameters, including SIR-qMT, T_2 and ADC, were fitted on a pixel-wise basis. The SIR-qMT signal model described in Equations [1]–[3] has seven independent parameters: R_{1f}, R_{1m}, S_f, S_m, $M_{f\infty}$, PSR and k_{mf}. As shown in previous studies (19), R_{1m} can be set equal to R_{1f} because of the weak dependence of SIR signals on R_{1m}. To further enhance the simplicity of fitting, numerical simulations were performed to provide S_m as 0.83 for the 1-ms hard inversion pulse used in the current study (18). Therefore, five parameters, i.e. R_{1f}, S_f, $M_{f\infty}$, PSR and k_{mf}, were fitted from SIR-EPI data using a least-squares method. The spin–lattice relaxation time T_1 was calculated simultaneously. Regions of interest (ROIs) of tumor, gray matter (GM) and white matter (WM) were manually selected from the T_1 map of each rat, and ROI-based group analyses were also performed to investigate the feasibility of using qMT parameters to differentiate between different types of tissue.

Computer simulations

To investigate the influence of the saturation echo train, B_1 inhomogeneity and relaxation times on the fitted qMT parameters, computer simulations were performed by solving six coupled differential equations (12). The simulations mimicked the actual imaging experiments, so that all pulse sequence parameters, including the 20 inversion times, were the same as those used in the actual MRI scanning. The intrinsic qMT and relaxation parameters were set to the experimentally fitted values (shown in Table 1), except that R_{2m} was 100 kHz (18).

RESULTS

Figure 2A shows eight SIR-EPI images of a representative rat from a total of 16 images with different inversion times. The SIR signals of four typical ROIs, i.e. GM, WM, tumor and contralateral normal brain tissue, and the corresponding fitted curves obtained using Equations [1]–[3] are shown in Fig. 2B. All signals were normalized by the corresponding signals at the longest inversion time of 10 s. For visualization purposes, a magnified image with short (<250 ms) inversion times is inserted in Fig. 2B, which shows

Table 1. Summary of region of interest (ROI)-based parameter means ± standard deviations of all animals

	R_1 (Hz)	R_2 (Hz)	ADC (μm²/ms)	PSR (%)	k_{mf} (Hz)	k_{fm} (Hz)
Tumor	0.47 ± 0.07	27.42 ± 2.22	0.80 ± 0.10	5.67 ± 0.95	19.69 ± 2.88	1.10 ± 0.15
GM	0.59 ± 0.05	24.91 ± 0.26	0.68 ± 0.03	9.20 ± 0.86	14.82 ± 2.12	1.35 ± 0.16
WM	0.63 ± 0.03	29.33 ± 2.08	0.79 ± 0.13	17.42 ± 2.05	10.23 ± 0.99	1.77 ± 0.19

ADC, apparent diffusion coefficient; PSR, pool size ratio.
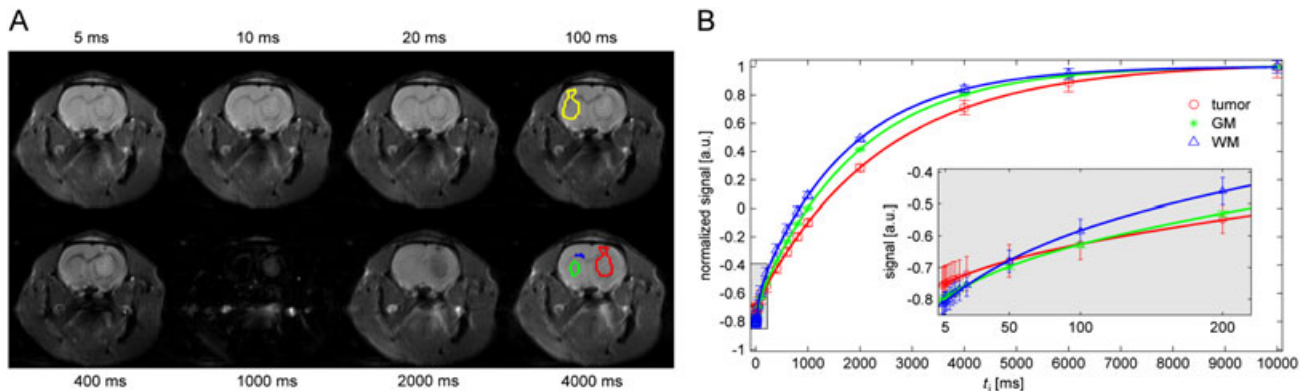
Figure 2. (A) Eight representative selective inversion recovery-echo planar imaging (SIR-EPI) images from a total of 20 images with different inversion times. The region of interest (ROI) boundaries of subcortical gray matter (green), corpus callosum white matter (blue), tumor (red) and contralateral normal tissue (yellow) are overlaid on the images. (B) The corresponding model fits of SIR signals normalized by the corresponding signals at $t_i = 10$ s. A magnified image with a logarithmic axis of inversion time is inserted to show the excellent agreement between the SIR-quantitative magnetization transfer (qMT) data (open markers) and the bi-exponential model of Equation [1] (full lines) at short inversion times. The error bars represent the standard deviations of ROI.

excellent agreement between the SIR-qMT data (open symbols) and the bi-exponential recovery model of Equations [1]–[3] (full lines). It is clear that the tumor shows a very different bi-exponential recovery behavior, in addition to its different recovery rate R_1.

Figure 3 shows representative parametric maps overlaid on a corresponding spin-echo EPI image. All parameters, T_1, T_2, ADC, PSR, k_{mf} and k_{fm}, provide clear imaging contrast to differentiate tumor, GM and WM tissues, although the overall k_{mf} and k_{fm} maps are much more noisy, as found previously (20). For a clear comparison, Table 1 summarizes all ROI-based parameter means and their standard deviations for all animals. As expected from multiple earlier studies, T_1 was significantly increased in tumor. However, by contrast, T_2 was found to be lower in the 9 L tumor region at this field, which is opposite to previous observations at 4.7 T (30). ADC was higher in the tumor region, suggesting a lower cellularity compared with normal tissues. PSR was

significantly lower in the tumor, which is consistent with a few previously reported observations that used different qMT acquisition methods (8,23–25). The k_{mf} and k_{fm} maps show clear contrast between GM and WM and higher values within the tumor, but the overall signal-to-noise ratios are much lower.

Figure 4 shows pixel-wise correlations between SIR-qMT parameters (PSR, k_{mf} and k_{fm}) and conventional MRI parameters ($R_1 = 1/T_1$, $R_2 = 1/T_2$ and ADC) from a representative rat. It is clear that PSR shows strong correlations with conventional MRI parameters, i.e. R_1 and R_2, with $p < 0.01$ in Pearson's correlation. Interestingly, although the MT exchange rates, k_{mf} and k_{fm}, show significant correlations with R_1 and ADC, there is no significant correlation between k_{mf}/k_{fm} and R_2 ($p = 0.08$ and $p = 0.27$, respectively). It should be noted that increasing PSR correlates positively with R_1 but negatively with R_2, suggesting that the factors dominating R_2 differ from those affecting R_1. A similar
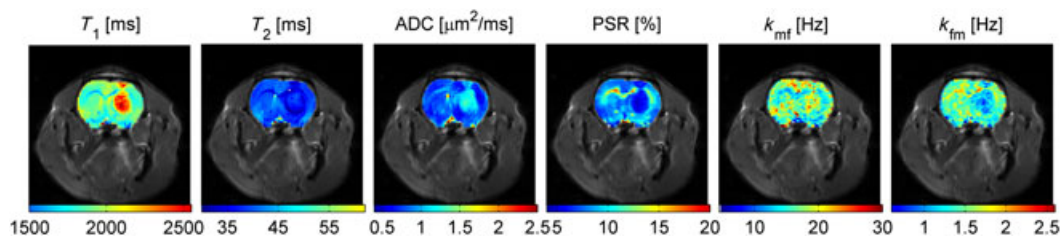
Figure 3. Representative multiple parametric maps overlaid on a corresponding spin-echo echo planar imaging (EPI) image. The pool size ratio (PSR) provides excellent differentiation of tumor, gray matter and white matter tissues. Although there is a clear contrast between gray matter and white matter, the overall k_{mf} and k_{fm} maps are much noisier.
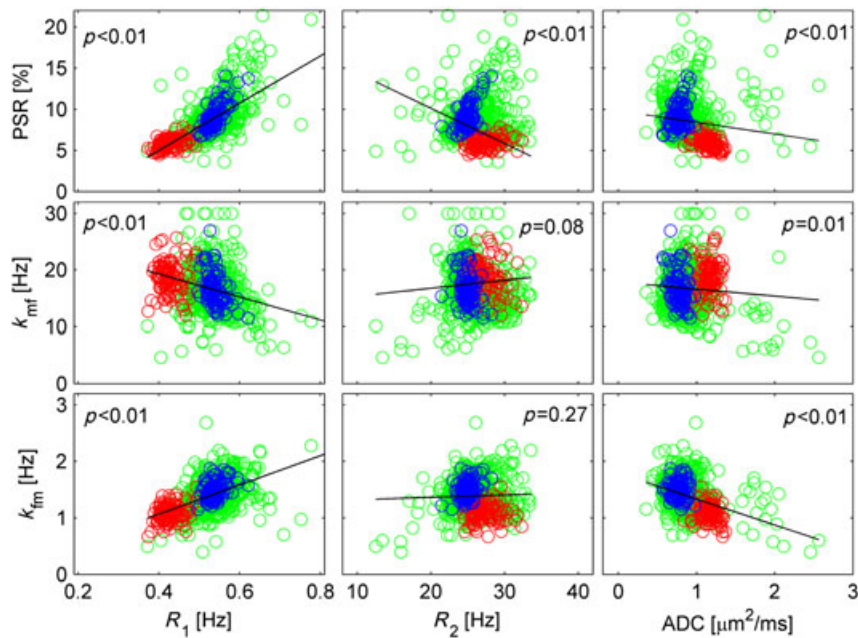
Figure 4. Pixel-wise correlations between selective inversion recovery-quantitative magnetization transfer (SIR-qMT) parameters [pool size ratio (PSR), k_{mf} and k_{fm}] and conventional MRI parameters [R_1, R_2 and apparent diffusion coefficient (ADC)]. Red circles represent pixels inside the tumor, blue those in the contralateral normal tissue and green for all other brain tissue. The p values of Pearson's correlation of all pixels in each subfigure are provided, and a corresponding linear regression fit is shown as the black full lines.

analysis was performed on all other rats and similar results were observed (data not shown).

Figure 5 summarizes the results of measured PSR and MT exchange rates in ROIs in all eight rats. Balanced one-way analyses of variance suggested that the mean differences in qMT parameters, i.e. PSR, k_{mf} and k_{fm}, of different tissue types were highly significant ($p < 10^{-12}$, $p < 10^{-7}$ and $p < 10^{-6}$, respectively). In addition, a multiple comparison procedure with Bonferroni correction was performed to evaluate the difference between each pair of tissues, and the corrected p values are given in Table 2. All Bonferroni-corrected p values are much smaller than 0.05, suggesting that all three qMT parameters provide highly reliable ways to differentiate between tissue types. For comparison, previously reported (19) PSR and k_{mf} values of a healthy rat

using the SIR-qMT method were PSR = 0.080 ± 0.008 in GM and 0.173 ± 0.023 in WM, and k_{mf} = 20.8 ± 6.5 Hz in GM and 13.1 ± 2.9 Hz in WM. Therefore, although k_{mf} values are slightly different in the current work, our fitted MR parameters were in good agreement with previous results. For qMT parameters in tumor, PSR was measured to be 0.040 ± 0.002 in C6 gliomas using the pulsed saturation qMT method (25), which is close to the PSR of 9 L tumors obtained in the current study using the SIR-qMT method, and both are significantly lower than those of normal tissue.

Figure 6 shows the influence of the saturation echo train, B_1 inhomogeneity and relaxation times on the fitted qMT parameters. At $\Delta B_1 = 0$ (i.e. perfect RF pulses), the fitted PSRs of all three types of tissue have <3.5% relative differences from the intrinsic values, suggesting that the saturation echo train used in the current SIR-EPI sequence has little influence on the estimates. Within ±20% errors of the B_1 field, the relative errors of the fitted PSR are within the range of +3.0% and −8.7% of the intrinsic values. However, k_{mf} seems to be insensitive to B_1 inhomogeneity (<1.1% different from the intrinsic value). k_{fm} was calculated from k_{mf} and PSR, and so the relative percentage errors of k_{fm} are similar to those of the fitted PSR values. Interestingly, the percentage errors of all fitted qMT parameters of three different types of tissue are similar to each other despite the significant difference in
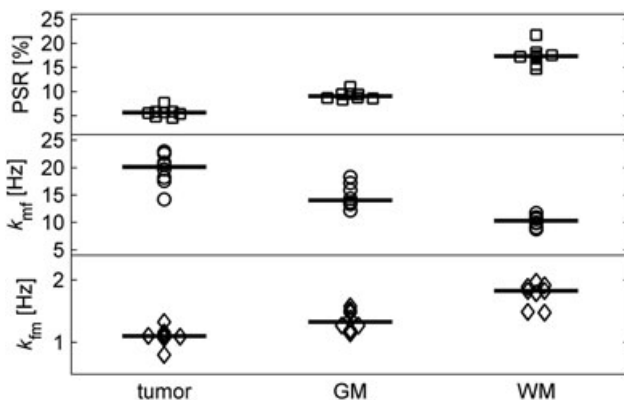
Figure 5. Summary of fitted pool size ratio (PSR), k_{mf} and k_{fm} [magnetization transfer (MT) exchange rates] of all eight animals. All parameters can differentiate different types of tissue, i.e. tumor, gray matter (GM) or white matter (WM), with statistical significance ($p < 10^{-12}$, $p < 10^{-7}$ and $p < 10^{-8}$, respectively), given by balanced one-way analyses of variance).

Table 2. Bonferroni-corrected p values for all pairwise comparisons in Fig. 5

	Tumor *versus* GM	Tumor *versus* WM	GM *versus* WM
PSR	1.83×10^{-6}	5.25×10^{-8}	1.22×10^{-6}
k_{mf}	0.012	3.91×10^{-5}	4.80×10^{-4}
k_{fm}	0.008	5.79×10^{-5}	3.45×10^{-4}

GM, gray matter; PSR, pool size ratio; WM, white matter.
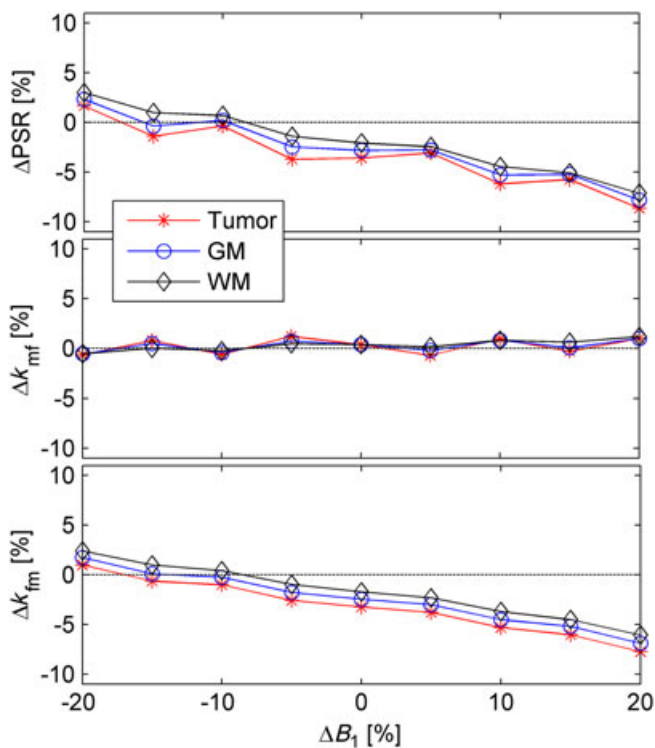
Figure 6. Simulated relative errors of quantitative magnetization transfer (qMT) parameters with the presence of saturation echo train, B_1 inhomogeneity and different relaxation times. Note that $k_{fm} = k_{mf} \times$ PSR. GM, gray matter; PSR, pool size ratio; WM, white matter.

relaxation times. This suggests that the parameter fitting depicted in Equations [1]–[3] is robust in the face of variations of other confounding factors in practice.

DISCUSSION

This study demonstrates the feasibility of performing SIR-qMT measurements in tumors *in vivo*, and provides insights into the biophysical changes that characterize 9 L tumors in rats. Although MTR has been widely used in cancer studies, only a few qMT imaging studies of tumors have been reported using the pulsed saturation method, and the SIR-qMT method has not been applied previously to tumors. Compared with the pulsed saturation qMT method, the SIR-qMT method has a significant shortcoming in that multi-slice imaging is difficult (although three-dimensional approaches are feasible) because the refocusing pulses in the saturation train can cause MT effects in neighboring slices (20). However, the SIR-qMT method has advantages when only a few slices are required for a limited coverage, e.g. tumors. As T_1 and MT parameters can be obtained simultaneously, the SIR-qMT method might be a promising technique to perform qMT cancer imaging. In addition, pulsed saturation and steady-state free-precession based qMT approaches may be difficult to implement on high-field human scanners because of RF power limitations and magnetic field inhomogeneities, whereas the SIR-qMT technique can be implemented at ultrahigh field strength for higher signal-to-noise ratio (20).

In the previous qMT imaging of tumors, Underhill *et al.* (25) used a different rodent glioma C6 model, but also found a significant decrease in PSR in tumors. Interestingly, they also found

that tumors had lower ADCs in their study, suggesting a higher cellular density without increased macromolecular content compared with normal brain tissue, consistent with earlier studies of higher water content in tumor cells (31). However, in the current study, ADC was found to be higher in the 9 L tumor, which has also been reported previously (27). Although several other factors may also affect the ADC of tissue, the above observations may indicate that a tumor may have a higher or lower cellularity depending on different tumor types and/or different stages. However, whatever the value of the ADC, all of the above studies showed that PSR in tumor is significantly lower than that in normal tissue. The agreement with previous studies suggests that the macromolecular content is more dilute in rapidly growing tissues and tumors, and is consistent with the conventional explanation for increased values of T_1 in tumors (32). The finding that T_2 is shorter in tumors is, at first sight, anomalous, and disagrees with a large body of earlier literature (33), but those studies were performed at substantially lower fields. Moreover, lower PSR would predict that T_2 would also be longer, as found for T_1, as long as the same mechanisms of relaxation are dominant for both longitudinal and transverse relaxations. Clearly, this cannot be the case, but the paradox is resolved if the dominant relaxation process for T_2 relaxation is chemical exchange rather than dipole–dipole interactions. We have shown previously that the relaxivity of diamagnetic proteins increases dramatically at high fields as chemical exchange contributions take over from other processes (34), and, in the case of our 9 L tumor, it appears that the relaxation efficacy of the macromolecular content increases more than the amount of solid material decreases. One way in which this can occur is if the rate of exchange (or the chemical shift difference) between exchanging protons and water increases in tumors. Such an effect can arise if, for example, there are appropriate changes in pH or protein degradation. This conclusion is further validated by the apparent increase in the rate of MT k_{mf}, which indicates that there is much faster transfer of magnetization from macromolecules to water in tumors relative to normal tissues.

These findings are relevant for the interpretation of other studies, such as CEST imaging of tumors. CEST provides molecular imaging contrast and detects endogenous mobile molecules with high spatial resolution, and has shown potential for the detection of cancer (33) and monitoring of the tumor response to treatment (35). Our results suggest that an increase in CEST in tumors may not reflect an increase in macromolecular content, but rather an increased rate of exchange and longer T_1 values, which has been found previously (36).

Although the precise mechanism of MT in tumors is not fully understood, both current and previous studies have suggested that PSR in tumors is significantly lower than that in normal brain tissues. QMT measurements may potentially provide more specific information on the content of the tumor microenvironment relative to relaxation times alone. Moreover, qMT may also potentially be useful for the detection of changes in tumors following certain treatments, if they cause significant changes in macromolecular content, such as increases in the development of polyploidy (37) or decreases during apoptosis (38).

The saturation echo train in the current study significantly reduces the total acquisition time, but only induces a small error to the fitted qMT parameters. More RF pulses in the saturation echo train can further reduce the induced errors, but this, in turn, will increase the scanning time and, more importantly, increase the specific absorption rate, which could be a problem for

NMR IN BIOMEDICINE

high-field clinical studies. With ±20% errors of the ideal B_1 field, the simulations show that the fitted PSR has <8.7% errors, whereas k_{mf} has <1.1% errors. This suggests that the SIR-EPI method is a reliable means to measure qMT parameters in practice. The fact that the fitted qMT parameters are insensitive to relaxation times is encouraging, which shows that SIR-EPI can provide robust measurements of qMT parameters despite the significant relaxation variations in tumors or other lesions.

Altogether, 20 different inversion times (t_i) were used in the current work and the pre-delay time t_d was kept constant. Such a scheme provides an excellent fitting of bi-exponential recovery signals, but requires a longer scanning time. It is possible to use the Cramer–Rao lower bound method to optimize both t_i and t_d in order to achieve a minimum scanning time. We have shown previously that only five measurements are required to fit SIR-qMT data in a healthy rat if T_1 is in the range 0.67–2 s (19). Tumors have significantly different T_1 relaxation times and MT parameters, such as $T_1 \sim 2.3$ s in this study. Hence, the previously optimized parameters may not be appropriate for the imaging of tumor-bearing rats. A new optimization which covers a larger range of T_1 and MT parameters is currently under development to speed up future SIR-qMT measurements in cancer imaging.

CONCLUSIONS

SIR-qMT has been implemented in a rodent glioma model for the first time. All signals were explained well by the bi-exponential recovery model. The fitted quantitative MT parameters suggest that tumor has significantly lower macromolecular contents and a higher MT exchange rate, which are consistent with previously reported results. This suggests that SIR-qMT can potentially serve as an imaging biomarker to detect changes in the microenvironment in tumor, and hence potentially may be able to monitor tumor response to treatment. These results also assist in the clarification of the contrast reported in the CEST imaging of tumors.

REFERENCES

1. Wolff SD, Balaban RS. Magnetization transfer contrast (MTC) and tissue water proton relaxation in vivo. Magn. Reson. Med. 1989; 10 (1): 135–144.
2. Filippi M, Rocca MA. Magnetization transfer magnetic resonance imaging in the assessment of neurological diseases. J. Neuroimaging, 2004; 14(4): 303–313.
3. Aisen AM, Doi K, Swanson SD. Detection of liver fibrosis with magnetic cross-relaxation. Magn. Reson. Med. 1994; 31(5): 551–556.
4. McDaniel JD, Ulmer JL, Prost RW, Franczak MB, Jaradeh S, Hamilton CA, Mark LP. Magnetization transfer imaging of skeletal muscle in autosomal recessive limb girdle muscular dystrophy. J. Comput. Assist. Tomogr. 1999; 23(4): 609–614.
5. Niemi P, Kurki T, Lundbom N, Kormano M. Magnetization transfer contrast in Gd-DTPA-enhanced imaging of brain tumors. Invest. Radiol. 1991; 26(Suppl. 1): S248–S249; discussion S253–S254.
6. Li W, Zhang Z, Nicolai J, Yang GY, Omary RA, Larson AC. Magnetization transfer MRI in pancreatic cancer xenograft models. Magn. Reson. Med. 2012; 68(4): 1291–1297.
7. Abramson RG, Arlinghaus LR, Weis JA, Li X, Dula AN, Chekmenev EY, Smith SA, Miga MI, Abramson VG, Yankeelov TE. Current and

8. Quesson B, Bouzier AK, Thiaudiere E, Delalande C, Merle M, Canioni P. Magnetization transfer fast imaging of implanted glioma in the rat brain at 4.7 T: interpretation using a binary spin-bath model. J. Magn. Reson. Imaging, 1997; 7(6): 1076–1083.
9. Kumar V, Jagannathan NR, Kumar R, Thulkar S, Gupta SD, Hemal AK, Gupta NP. Evaluation of the role of magnetization transfer imaging in prostate: a preliminary study. Magn. Reson. Imaging, 2008; 26(5): 644–649.
10. Barker GJ, Schreiber WG, Gass A, Ranjeva JP, Campi A, van Waesberghe JH, Franconi JM, Watt HC, Tofts PS. A standardised method for measuring magnetisation transfer ratio on MR imagers from different manufacturers—the EuroMT sequence. MAGMA, 2005; 18(2): 76–80.
11. Tofts PS, Steens SC, Cercignani M, Admiraal-Behloul F, Hofman PA, van Osch MJ, Teeuwisse WM, Tozer DJ, van Waesberghe JH, Yeung R, Barker GJ, van Buchem MA. Sources of variation in multi-centre brain MTR histogram studies: body-coil transmission eliminates inter-centre differences. MAGMA, 2006; 19(4): 209–222.
12. Henkelman RM, Huang XM, Xiang QS, Stanisz GJ, Swanson SD, Bronskill MJ. Quantitative interpretation of magnetization-transfer. Magn. Reson. Med. 1993; 29(6): 759–766.
13. Gochberg DF, Kennan RP, Gore JC. Quantitative studies of magnetization transfer by selective excitation and T-1 recovery. Magn. Reson. Med. 1997; 38(2): 224–231.
14. Sled JG, Pike GB. Quantitative interpretation of magnetization transfer in spoiled gradient echo MRI sequences. J. Magn. Reson. 2000; 145(1): 24–36.
15. Gochberg DF, Fong PM, Gore JC. A quantitative study of magnetization transfer in MAGIC gels. Phys. Med. Biol. 2003; 48(21): N277–N282.
16. Edzes HT, Samulski ET. The measurement of cross-relaxation effects in the proton NMR spin–lattice relaxation of water in biological systems: hydrated collagen and muscle. J. Magn. Reson. 1978; 31 (2): 207–229.
17. Gochberg DF, Gore JC. Quantitative imaging of magnetization transfer using an inversion recovery sequence. Magn. Reson. Med. 2003; 49(3): 501–505.
18. Gochberg DF, Gore JC. Quantitative magnetization transfer imaging via selective inversion recovery with short repetition times. Magn. Reson. Med. 2007; 57(2): 437–441.
19. Li K, Zu Z, Xu J, Janve VA, Gore JC, Does MD, Gochberg DF. Optimized inversion recovery sequences for quantitative T1 and magnetization transfer imaging. Magn. Reson. Med. 2010; 64(2): 491–500.
20. Dortch RD, Li K, Gochberg DF, Welch EB, Dula AN, Tamhane AA, Gore JC, Smith SA. Quantitative magnetization transfer imaging in human brain at 3 T via selective inversion recovery. Magn. Reson. Med. 2011; 66(5): 1346–1352.
21. Dortch RD, Moore J, Li K, Jankiewicz M, Gochberg DF, Hirtle JA, Gore JC, Smith SA. Quantitative magnetization transfer imaging of human brain at 7 T. Neuroimage, 2013; 64: 640–649.
22. Li K, Dortch RD, Bryant ND, Buck AKW, Towse TF, Gochberg DF, Does MD, Damon BM, Park JH. In vivo transverse relaxation and magnetization transfer imaging of human thigh muscles at 3.0 Tesla. *Proceedings of the 22nd Annual Meeting ISMRM*, Salt Lake City, UT, USA, 2013; 3508.
23. Yarnykh VL. Pulsed Z-spectroscopic imaging of cross-relaxation parameters in tissues for human MRI: theory and clinical applications. Magn. Reson. Med. 2002; 47(5): 929–939.
24. Tozer DJ, Rees JH, Benton CE, Waldman AD, Jager HR, Tofts PS. Quantitative magnetisation transfer imaging in glioma: preliminary results. NMR Biomed. 2011; 24(5): 492–498.
25. Underhill HR, Rostomily RC, Mikheev AM, Yuan C, Yarnykh VL. Fast bound pool fraction imaging of the in vivo rat brain: association with myelin content and validation in the C6 glioma model. Neuroimage, 2011; 54(3): 2052–2065.
26. van Zijl PC, Yadav NN. Chemical exchange saturation transfer (CEST): what is in a name and what isn't? Magn. Reson. Med. 2011; 65(4): 927–948.
27. Colvin DC, Yankeelov TE, Does MD, Yue Z, Quarles C, Gore JC. New insights into tumor microstructure using temporal diffusion spectroscopy. Cancer Res. 2008; 68(14): 5941–5947.

28. Hu X, Le TH. Artifact reduction in EPI with phase-encoded reference scan. Magn. Reson. Med. 1996; 36(1): 166–171.

29. Maes F, Collignon A, Vandermeulen D, Marchal G, Suetens P. Multimodality image registration by maximization of mutual information. IEEE Trans. Med. Imaging, 1997; 16(2): 187–198.

30. Rajan SS, Rosa L, Francisco J, Muraki A, Carvlin M, Tuturea E. MRI characterization of 9 L-glioma in rat brain at 4.7 Tesla. Magn. Reson. Imaging, 1990; 8(2): 185–190.

31. Cramer W. On the biochemical mechanism of growth. J. Physiol. 1916; 50(5): 322–334.

32. Saryan LA, Hollis DP, Economou JS, Eggleston JC. Nuclear magnetic resonance studies of cancer. IV. Correlation of water content with tissue relaxation times. J. Natl. Cancer Inst. 1974; 52(2): 599–602.

33. Zhou J, Lal B, Wilson DA, Laterra J, van Zijl PC. Amide proton transfer (APT) contrast for imaging of brain tumors. Magn. Reson. Med. 2003; 50(6): 1120–1126.

34. Zhong JH, Gore JC, Armitage IM. Relative contributions of chemical exchange and other relaxation mechanisms in protein solutions and tissues. Magn. Reson. Med. 1989; 11(3): 295–308.

35. Wang S, Tryggestad E, Zhou T, Armour M, Wen Z, Fu DX, Ford E, van Zijl PC, Zhou J. Assessment of MRI parameters as imaging biomarkers for radiation necrosis in the rat brain. Int. J. Radiat. Oncol. Biol. Phys. 2012; 83(3): e431–e436.

36. Xu J, Zu Z, Zaiss M, Xie J, Gochberg DF, Bachert P, Gore JC. On the origins of chemical exchange saturation transfer (CEST) contrast in tumors at 9.4T. NMR Biomed. in press.

37. Xu J, Li K, Smith RA, Waterton JC, Zhao P, Chen H, Does MD, Manning HC, Gore JC. Characterizing tumor response to chemotherapy at various length scales using temporal diffusion spectroscopy. PLoS ONE, 2012; 7(7): e41714.

38. Bailey C, Desmond KL, Czarnota GJ, Stanisz GJ. Quantitative magnetization transfer studies of apoptotic cell death. Magn. Reson. Med. 2011; 66(1): 264–269.